Journal of Biomedical Optics

BiomedicalOptics.SPIEDigitalLibrary.org

Quantitative phase imaging through scattering media by means of coherence-controlled holographic microscope

Vera Kollarova
Jana Collakova
Zbynek Dostal
Pavel Vesely
Radim Chmelik

SPIE.

Quantitative phase imaging through scattering media by means of coherence-controlled holographic microscope

Vera Kollarova,[a,*] Jana Collakova,[a,b] Zbynek Dostal,[a,b] Pavel Vesely,[a] and Radim Chmelik[a,b]
[a]Brno University of Technology, CEITEC—Central European Institute of Technology, Technicka 3058/10, Brno 616 00, Czech Republic
[b]Brno University of Technology, Institute of Physical Engineering, Faculty of Mechanical Engineering, Technicka 2896/2, Brno 616 00, Czech Republic

Abstract. A coherence-controlled holographic microscope (CCHM) enables quantitative phase imaging with coherent as well as incoherent illumination. The low spatially coherent light induces a coherence gating effect, which makes observation of samples possible also through scattering media. The paper describes theoretically and simulates numerically imaging of a two-dimensional object through a static scattering layer by means of CCHM, with the main focus on the quantitative phase imaging quality. The authors have investigated both strongly and weakly scattering media characterized by different amounts of ballistic and diffuse light. It is demonstrated that the phase information can be revealed also for the case of the static, strongly scattering layer. The dependence of the quality of imaging process on the spatial light coherence is demonstrated. The theoretical calculations and numerical simulations are supported by experimental data gained with a model phase object, as well as living carcinoma cells treated in an optically turbid emulsion. [DOI: 10.1117/1.JBO.20.11.111206]

Keywords: quantitative phase imaging; digital holography; microscopy; coherence-controlled holographic microscopy; imaging through scattering media; imaging through turbid media.

Paper 150156SSPR received Mar. 13, 2015; accepted for publication Jul. 1, 2015; published online Aug. 5, 2015.

1 Introduction

Imaging through scattering media is an important task in biomedical as well technical research and applications. It is solved by various methods based on, e.g., wavefront shaping,[1,2] speckle correlations,[3,4] inverse scattering,[5] time gating,[6,7] or optical coherence tomography,[8] which can reveal information about the object.

In recent decades, digital holographic microscopy based on transmission mode has made quantitative phase imaging (QPI) of living cells and other phase objects[9–13] possible, and its potential and applications are further investigated. At the same time, it has been demonstrated that digital holography makes possible imaging of objects also through scattering media. The techniques are often based on a coherence gating effect and utilization of ballistic light. The aim is to sort out nonscattered (ballistic) or slightly scattered (snake-like) light to construct a high-quality image, e.g., using the first arriving light method for pulse lasers[14] or spatial filtering of c-w lasers with coherent light.[15] Recently, the possibility of imaging by means of a coherent light through a flowing turbid medium based on a Doppler frequency shift[16] and through a quasistationary turbid medium by multiple holographic acquisitions was studied.[17] A combination of digital holography with two-point intensity correlation[18] or phase-shifting digital holography using temporally low-coherence light[19] to recover the phase information through a scattering medium was also presented.

Imaging through scattering media is possible also by means of spatially incoherent light as reported by Leith.[14] The coherence-controlled holographic microscope[20] (CCHM) makes possible imaging through a flowing turbid as well as static scattering medium D by means of the spatially incoherent light, utilizing ballistic and diffuse light. The microscope is a two-arm, off-axis holographic system with a halogen lamp as a source [see Fig. 1(a)]. The temporal and spatial coherence of light can be modified by interference filter IF and by a changeable size of an aperture A. Thus, the quality of the image information can also be changed. The system is particularly used in the spatially incoherent regime. Besides the benefits of better resolution and no speckles in the image,[20] observation through a scattering layer or medium is then possible due to the coherence gating effect.[21] A point object imaging through a diffuse layer was theoretically described recently.[21,22] It was shown that the image can be taken only locally invariant.[22] The experiments were carried out with an amplitude object, and it was demonstrated that the imaging of a two-dimensional (2-D) amplitude object is possible not only by means of ballistic light, but also by means of diffuse (scattered) light.[21] However, neither theoretical nor experimental study of the influence of the scattering layer on the phase information was performed and discussed.

This paper proves the possibility of QPI of 2-D phase objects through a static phase scattering layer by means of CCHM. The imaging of an object with defined phase is numerically as well as experimentally evaluated for weak and strong diffuse layers. The paper shows that the phase values can be quantitatively reconstructed, however, in some cases in a restricted region

*Address all correspondence to: Vera Kollarova, E-mail: vera.kollarova@ceitec.vutbr.cz

only. The authors demonstrate here the benefits of the spatially incoherent light for the imaging, especially for the case of strong diffusers. Finally, a time-lapse experiment with a 4-mm-thick layer of turbid medium demonstrates the possibility to observe living cells through scattering media.

2 Two-Dimensional Object Imaging Through a Scattering Layer—Mathematical Description

The three-dimensional imaging properties of the CCHM [Fig. 1(a)] have been already presented in detail.[22] The optical model was simplified in the calculations; only the condenser and objective lenses were assumed. The calculations were based on the Fourier optics concept, assuming elastic and linear scattering. Moreover, a point object imaging through a thin 2-D diffuse layer was discussed there in the parabolic approximation.

This study investigates observation of a 2-D object placed in front of a thin diffuse layer, in the parabolic approximation. The light is supposed to be quasi-monochromatic with a central wavelength λ, however spatially incoherent. According to the microscope arrangement, interference of the object and reference beams is recorded at the output plane. The information about the object amplitude and phase is carried in the mixed term of the interference law.[22]

According to Chmelik et al.,[22] imaging of a single point placed in the position $\mathbf{r}_{St} = (x_S, y_S)$ at the object plane through a single, thin scattering layer at a distance z_D behind the object plane [Fig. 1(b)] can be expressed by the function

$$w_D(\mathbf{r}_t, \mathbf{r}_{St}, z_D, \mathbf{r}_f) = s^*(\mathbf{r}_t - \mathbf{r}_{St}) p_D(\mathbf{r}_t, \mathbf{r}_{St}, z_D, \mathbf{r}_f). \quad (1)$$

Vector $\mathbf{r}_t = (x, y)$ represents coordinates in the output plane, and $\mathbf{r}_f = (x_f, y_f)$ is the mutual transverse shift of the images formed by the reference and object beam at the output plane, both reduced by objective magnification M. The symbol * denotes complex conjugation. Function $s(\mathbf{r}_t)$ depends on the optical properties of the reference arm and the coherence properties of the source.[22] It represents the mutual intensity function and can be approximated by the Bessel function of the first kind $J_1(\mu)$ for the case of waves propagating at small angles, when the pupil functions of lenses can be approximated by the circ function.[22] Then,

$$s(\mathbf{r}_t) = \frac{2J_1(\mu)}{\mu}, \quad (2)$$

with $\mu = 2\pi(\mathrm{NA}_S/\lambda)|\mathbf{r}_t|$. NA_S is the minimum of the numerical apertures of the source, condenser lens, and objective lens in the reference arm, and affects the degree of the spatial coherence. The width of the peak of $s(\mathbf{r}_t)$ decreases with increasing NA_S, which is equivalent to decrease of the spatial coherence. Function $p_D(\mathbf{r}_t)$ in Eq. (1) is related to imaging of the sample through the object arm and has the following form:[22]

$$p_D(\mathbf{r}_t, \mathbf{r}_{St}) = \iint_{-\infty}^{+\infty} p_0\left(\mathbf{r}_t - \mathbf{r}_{St} + \mathbf{Q}_{Dt}\frac{z_D}{K} - \mathbf{r}_f\right) T_D(\mathbf{Q}_{Dt}) \times \exp\left[-\mathrm{i}2\pi z_D \frac{|\mathbf{Q}_{Dt}|^2}{2K} + \mathrm{i}2\pi \mathbf{Q}_{Dt}\cdot\mathbf{r}_{St}\right] \mathrm{d}^2\mathbf{Q}_{Dt}. \quad (3)$$

According to Chmelik et al.,[22] the function $p_0(\mathbf{r}_t)$ is for the assumption of small angles propagation described by $p_0(\mathbf{r}_t) = [2J_1(\nu)]/\nu$, where $\nu = 2\pi(\mathrm{NA}/\lambda)|\mathbf{r}_t|$, NA is the numerical aperture of the objective lens in the object arm, and $K = 1/\lambda$. Function T_D represents the angular spectrum of the complex transmission function $t_D(\mathbf{r}_{Dt})$ of the 2-D diffuse layer defined by the Fourier transform

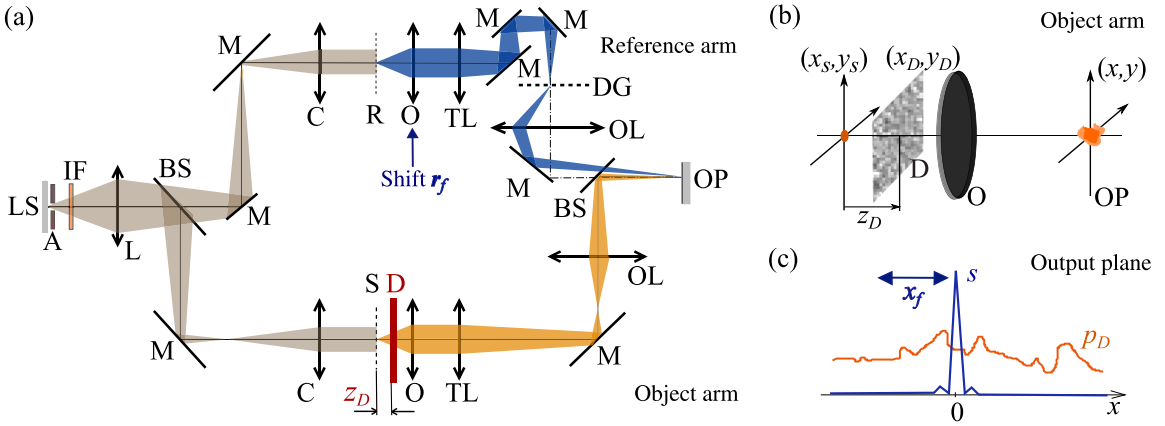

Fig. 1 (a) Scheme of the microscope: LS, light source; A, aperture of changeable size; IF, interference filter; L, collector lens; C, condenser lens; R, reference plane; S, sample (object) plane; D, diffuser; O, objective lens; TL, tube lens; DG, diffraction grating; OL, output lens; OP, output plane; BS, beam splitter; M, mirror; z_D, distance between the diffuser and the object plane; $\mathbf{r}_f$, transverse shift of the objective lens. (b) Simplified model of the imaging process through the object arm. A point object is imaged through the thin diffuse layer D by means of an objective lens O to the output plane. The position of the point object in the object plane is described by the coordinate vector $\mathbf{r}_{St} = (x_S, y_S)$; coordinates in the plane of the diffuser are $\mathbf{r}_{Dt} = (x_D, y_D)$; and coordinates in the output (image) plane reduced by objective magnification M are $\mathbf{r}_t = (x, y)$. The reference arm is optically identical, however, without the diffuser and object. (c) Function $s(\mathbf{r}_t)$ acts like a filter of $p_D(\mathbf{r}_t)$; the transverse shift $\mathbf{r}_f$ of $s(\mathbf{r}_t)$ makes it possible to change the profile of $w_D(\mathbf{r}_t)$ (see the text).

$$T_D(\mathbf{Q}_{Dt}) = \iint_{-\infty}^{+\infty} t_D(\mathbf{r}_{Dt}) \exp(\mathrm{i}2\pi\mathbf{Q}_{Dt} \cdot \mathbf{r}_{Dt}) \mathrm{d}^2\mathbf{r}_{Dt}. \quad (4)$$

Here, $\mathbf{Q}_{Dt}$ is a scattering vector of the diffuse layer and $\mathbf{r}_{Dt} = (x_D, y_D)$ is the vector of coordinates in the diffuser plane. According to Eqs. (1) and (3) and the diffuser properties defined by $t_D(\mathbf{r}_{Dt})$, the image w_D of a point object depends on the point object position $\mathbf{r}_{St}$.[22] The imaging is not spatially invariant; therefore, the function cannot be understood as an impulse response function. However, imaging can be considered to be locally isoplanatic (linear and spatially invariant). The stronger the scattering properties of the diffuse layer, the more significant the shape change of w_D and the smaller the region of its spatial invariance.

Imaging of a 2-D object defined by a transmission function $t_S(\mathbf{r}_{St})$ through a scattering layer can be described by the integral

$$u(\mathbf{r}_t) = \iint_{-\infty}^{+\infty} t_S(\mathbf{r}_{St}) w_D(\mathbf{r}_t, \mathbf{r}_{St}, z_D, \mathbf{r}_f) \mathrm{d}^2\mathbf{r}_{St}. \quad (5)$$

The mutual intensity $s(\mathbf{r}_t)$ [Eq. (2)] involved in w_D in Eq. (5) reflects the degree of spatial coherence. In the case of spatially incoherent light, $s(\mathbf{r}_t)$ exhibits a significant narrow peak and acts as a filter of function $p_D(\mathbf{r}_t)$ [see Eq. (1) and Fig. 1(c)]. The light from a certain object point therefore interferes only with the light from the corresponding point of the reference object plane (the so-called coherence gating effect). Due to it, the image can be created by ballistic (for $\mathbf{r}_f = 0$) as well as by diffuse light ($\mathbf{r}_f \neq 0$) in the presence of diffuse medium. In the case of a high spatial coherence, when $\mathrm{NA}_S \to 0$, the function $s(\mathbf{r}_t)$ is almost constant and equal to 1 and no filter effect occurs. The light from all points of the reference and image plane then interferes without restriction and speckles are created. The image of a single point object [Eq. (1)] is then determined by $p_D(\mathbf{r}_t)$ [Eq. (3)] completely.

3 Two-Dimensional Phase Object Imaging Through a Scattering Layer—Numerical Simulation

Numerical simulation of a 2-D phase object imaging through a scattering layer was based on Eq. (5). The function w_D in Eq. (1)

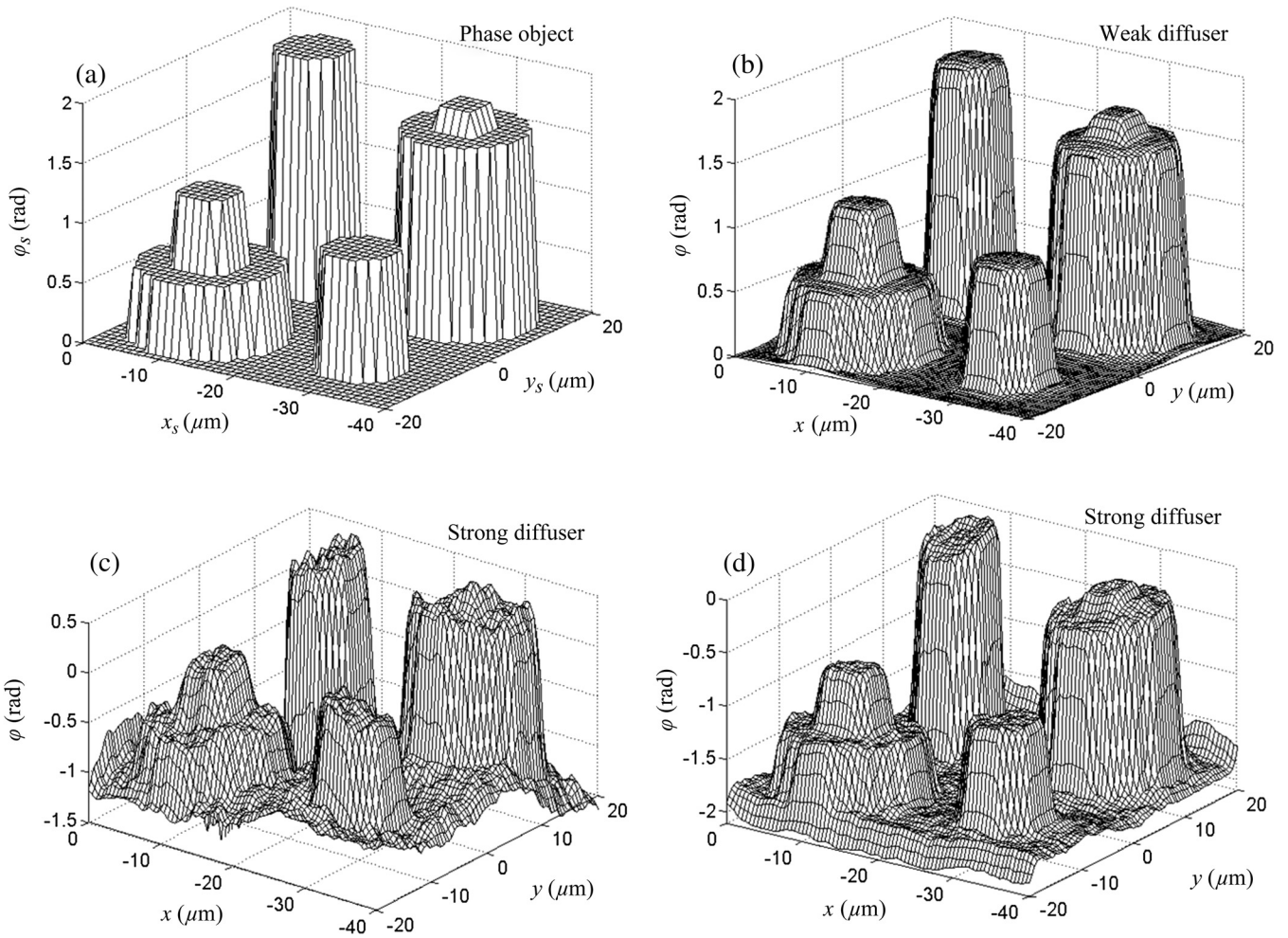

Fig. 2 Numerical simulation of reconstructed phase $\varphi = \arg(u)$ obtained by coherence-controlled holographic microscope, when a phase object $\varphi_s = \arg(t_s)$ (a) is imaged through a scattering layer placed 3 mm behind the layer. Phase image φ obtained (b) through a weak diffuser with $\sigma_D = 4\pi/5$ rad, (c) through a strong diffuser with $\sigma_D = 9\pi/5$ rad and zero transverse shift $\mathbf{r}_f = (0,0)$ μm, (d) through a strong diffuser with $\sigma_D = 9\pi/5$ rad and $\mathbf{r}_f = (26.5, 7.0)$ μm. The transverse shift $\mathbf{r}_f$ can significantly change the quality of the signal in the case of strong diffusors—compare (c) and (d).

was numerically calculated in MATLAB® for every point of the object plane and for the defined z_D and $\mathbf{r}_f$ (local invariance was not factored in). It represented a four-dimensional transmission matrix between the input and output planes. If necessary, the calculated phase of the image $u(\mathbf{r}_t)$ was unwrapped using the MATLAB® unwrap function. In case it failed, Goldstein unwrapping algorithm was used.[23]

The complex transmission function $t_D(\mathbf{r}_{Dt})$ of the diffuser was designed with regard to the diffuser properties used in the experimental part. It was modeled by a phase function defined by a matrix of $N \times N$ squared facets with the side length $d = \lambda/4$ and random phase shifts φ_{Djk}:

$$t_D(x_D, y_D) = \sum_{j=-J}^{J} \sum_{k=-J}^{J} \exp(\mathrm{i}\varphi_{Djk})\delta(x_D - jd)\delta(y_D - kd) * \mathrm{rect}\left(\frac{x_D}{d}\right)\mathrm{rect}\left(\frac{y_D}{d}\right). \quad (6)$$

The symbol * denotes a convolution here, $J = (N-1)/2$, and the rectangle function "rect" is defined as $\mathrm{rect}(x) = 1$ for $|x| < d/2$; $\mathrm{rect}(x) = 0.5$ for $|x| = d/2$; otherwise, it is zero. The phases φ_{Djk} generated randomly by the computer were characterized by a Gaussian statistical distribution with a standard deviation σ_D. It means that various diffuser realizations generated with the same σ_D were different. This study presents two diffusers simulated with $N = 800$, $\lambda = 0.65$ μm and defined by standard deviation $4\pi/5$ and $9\pi/5$ rad. They differ by the amount of ballistic and diffuse light. The first diffuser (denoted as a weak one) transmits a significant amount of the ballistic (unscattered) light with regard to the diffuse (scattered) light. The second diffuser (denoted as a strong one) scatters into all directions without preference of the ballistic light direction.

A numerical simulation of imaging of a 2-D object with the phase $\varphi_S = \arg[t_S(\mathbf{r}_{St})]$, Fig. 2(a), through a scattering layer placed $z_D = 3$ mm behind the object by means of CCHM is shown in Fig. 2. The authors considered numerical aperture of the objective lenses and of the source $\mathrm{NA} = \mathrm{NA}_S = 0.25$, $\lambda = 0.65$ μm. In Fig. 2(b), a weak diffuser with $\sigma_D = 4\pi/5$ rad is used and reconstructed phase $\varphi = \arg[u(\mathbf{r}_t)]$ is shown. In the case of weak diffusers, the ballistic (unscattered) light is significant in comparison to the diffuse light. Therefore, the best image is formed always by the ballistic light. The fine details of the image can be lost because of the signal-to-noise ratio decrease; however, the quality of the image is comparable to imaging without a diffuser and the image can be obtained without difficulties.

In contrast, the quality of imaging with ballistic and diffuse light is similar in the case of strong diffusers, and mostly so noisy that the phase cannot be unwrapped. However, a proper mutual shift $\mathbf{r}_f \neq 0$ of the images formed by the object and reference beam can induce significant improvement of the signal, as demonstrated in Fig. 2(d) in comparison to Fig. 2(c). Figures 2(c) and 2(d) represent the reconstructed phase image $\varphi = \arg[u(\mathbf{r}_t)]$ through a strong diffuser with $\sigma_D = 9\pi/5$ rad for the zero shift and $\mathbf{r}_f = (26.5, 7.0)$ μm, respectively.

The improvement of the image quality for $\mathbf{r}_f \neq 0$ happens if the function w_D [Eq. (1)] becomes more narrow and smooth, exhibiting a significant principal maximum with low side lobes; thus, leading to a good-quality function w_D. In the case of spatially incoherent light, the function s [Eq. (2)] has a significant principal maximum. Hence, the quality of w_D is determined by

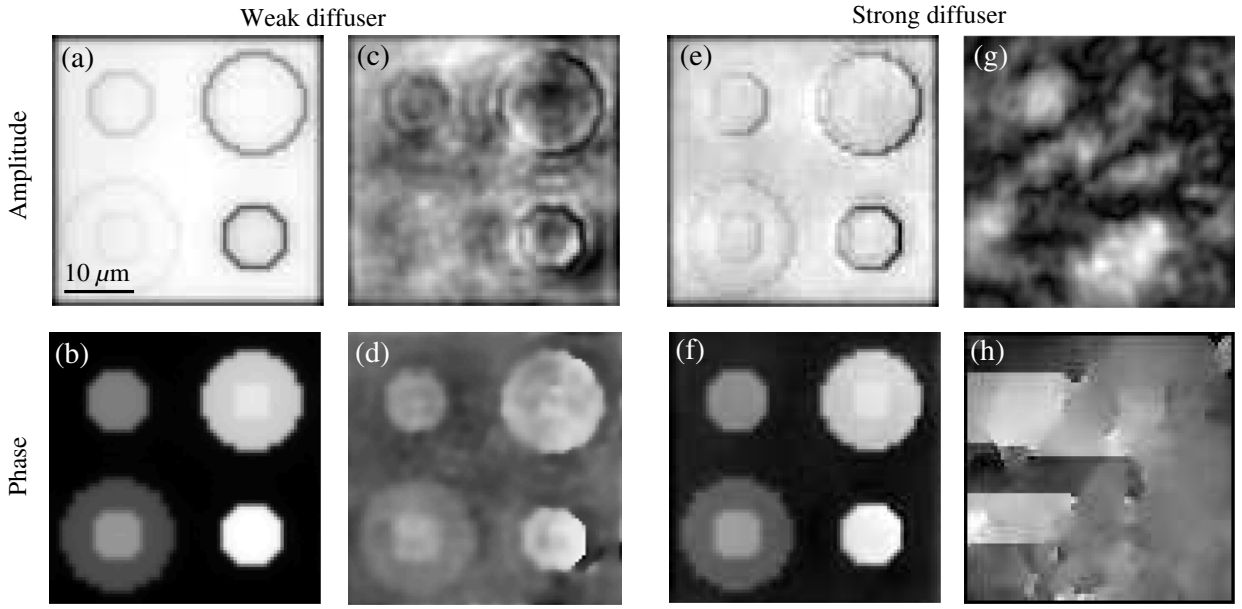

Fig. 3 Numerical simulation of the spatial coherence impact on the image amplitude $|u|$ and the image phase $\varphi = \arg(u)$ for $\mathrm{NA} = 0.25$, $z_D = 3$ mm. The object phase is represented by Fig. 2(a). (a) to (d) Images obtained through a weak diffuser with $\sigma_D = 4\pi/5$ rad: (a) reconstructed amplitude and (b) phase for spatially incoherent light characterized by $\mathrm{NA}_S = 0.25$; (c) reconstructed amplitude and (d) phase for almost spatially coherent light characterized by $\mathrm{NA}_S = 0.01$. (e) to (h) Images obtained through a strong diffuser with $\sigma_D = 9\pi/5$ rad and $\mathbf{r}_f = (26.5, 7.0)$ μm leading to the best reconstructed image quality, see Fig. 2(d). (e) Amplitude and (f) phase reconstruction for $\mathrm{NA}_S = 0.25$; (g) amplitude and (h) phase reconstruction for $\mathrm{NA}_S = 0.01$. Due to higher coherence noise, phase unwrapping is not successful in the case of spatially coherent light (h).

the shape of function p_D [Eq. (3)] and by the mutual shift $\mathbf{r}_f$ of the functions s and p. If there is at least a slightly significant direction of scattering $\mathbf{Q}_{Dtf}$ in T_D [Eq. (4)], p_D [Eq. (3)] exhibits a small local maximum in some position, see Fig. 1(c). A proper transverse shift $\mathbf{r}_f$ eliminates $\mathbf{Q}_{Dtf}z_D/K$ in Eq. (3) and leads to overlapping of s and p maxima and a good quality of the function w_D.

The good-quality function w_D can appear only in a part of the field of view, as will be demonstrated in Sec. 4. The phase can then be unwrapped at least in the relevant part of the image with the good-quality w_D. The improvement in the phase reconstruction is also reflected by the increase of the amplitude $|u(\mathbf{r}_t)|$. Finding the highest reconstructed amplitude image leads to the best possible phase reconstruction in the same region. For the nonzero shift $\mathbf{r}_f \neq 0$, the phase background is tilted according to Eqs. (1) and (3) and has to be compensated.

The effect of the degree of spatial coherence on the image quality due to the coherence gating effect is illustrated in Fig. 3. It demonstrates the decrease of image quality with increasing spatial coherence of the light in the presence of a diffuser for $z_D = 3$ mm. Figures 3(a)–3(d) represent imaging with a weak diffuser with $\sigma_D = 4\pi/5$ rad; Figs. 3(e)–3(h) represent imaging with a strong diffuser with $\sigma_D = 9\pi/5$ rad and the shift $\mathbf{r}_f = (26.5, 7.0)$ μm, leading to the best possible image quality for this diffuser realization (both diffusers are expressed by the same phase transmission function as in Fig. 2). The effect of the increasing spatial coherence of light on the amplitude $|u|$ is demonstrated in Figs. 3(a) and 3(c) for the weak diffuser and in Figs. 3(e) and 3(g) for the strong diffuser. The same effect on phase $\varphi = \arg(u)$ is simulated in Figs. 3(b) and 3(d), and Figs. 3(f) and 3(h) for the weak and strong diffusers, respectively. The low spatial coherence is determined by $\mathrm{NA}_S = 0.25$ for Figs. 3(a), 3(b), 3(e), and 3(f), and high spatial coherence by $\mathrm{NA}_S = 0.01$ for Figs. 3(c), 3(d), 3(g), and 3(h). In the case of high spatial coherence and a weak diffuser, Fig. 3(d) is affected by the coherence noise, the finer details are lost, and the phase unwrapping is a more complicated task. In case the MATLAB® unwrapping function failed, the Goldstein algorithm was successful. For the strong diffuser and high spatial coherence, the phase cannot be reconstructed, as clearly seen in Fig. 3(h). A similar situation also occurs for the weak diffuser if it is placed closer to the object. However, the low spatially coherent light makes QPI possible in all cases [see Figs. 3(b) and 3(f)]. The influence of noise on the phase reconstruction is discussed in more detail in Sec. 4.

4 Quantitative Phase Imaging Through a Scattering Layer—Experiments

The following experiments verify the possibility of quantitative phase imaging (QPI) through static scattering media by means of CCHM[20] [Fig. 1(a)]. A halogen lamp was used as a source, interference filter 650 nm with FWHM 10 nm (corresponding to the coherence length 42 μm), objective lenses $10\times/0.3$, and spatially incoherent light characterized by $\mathrm{NA}_S = 0.3$ [aperture A in Fig. 1(a) was fully open]. The optical magnification M between the object and image plane was 40×. The weak and strong diffusers in the form of a microroughened surface were created on one side of coverslips by different times of sandblasting and placed 0.8 mm behind the object. The phase object was formed in a glass coverslip by squares with defined depths leading to the phase shifts of 0.1, 0.35, 4, 6, and 8 rad for $\lambda = 650$ nm. In the first two columns of Table 1, the mean phase φ_m and the standard deviation σ of the phase values within the squares measured by means of the CCHM without a diffuser are summed. The surface of the sample was not smooth; therefore, σ is quite high.

Table 1 Comparison of the mean phase φ_m and the standard deviation σ of the phase values φ measured in the largest squares without and with a weak diffuser by means of a coherence-controlled holographic microscope.

Without diffuser		With a weak diffuser	
φ_m (rad)	σ (rad)	φ_m (rad)	σ (rad)
7.96	0.13	8.09	0.17
5.94	0.14	5.95	0.22
4.05	0.10	3.89	0.13
0.349	0.091	0.35	0.17
0.098	0.049	0.15	0.11

The obtained holograms were processed using the CCHM software, in which the Goldstein algorithm[23] was chosen to unwrap the reconstructed phase and the phase background was then compensated.[24] Although the phase shift of 8 rad is greater

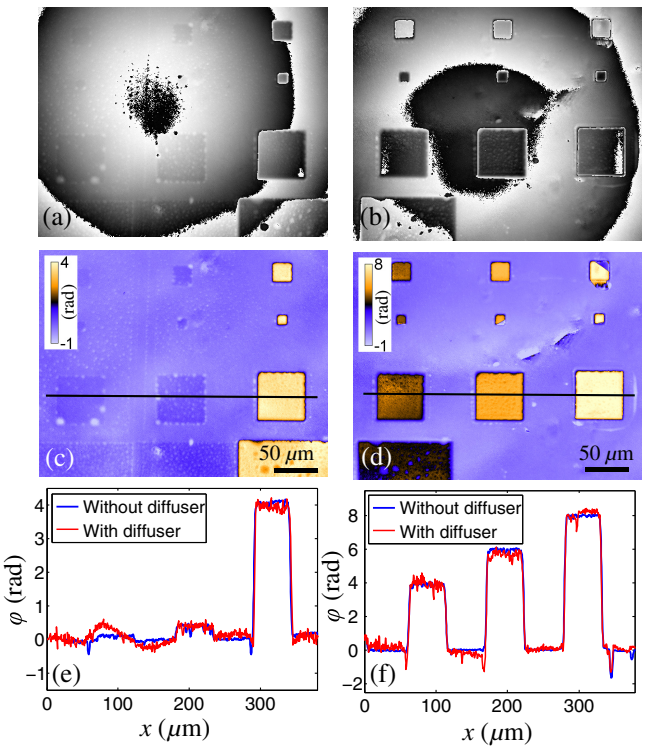

Fig. 4 Experimental verification of quantitative phase imaging (QPI) of square objects through a weak diffuser. (a) The wrapped and (c) compensated unwrapped phase image of squares with phase shifts of 0.1, 0.35, and 4 rad. (e) Comparison of the measured values along the black line in (c) with QPI values without the diffuser. (b) The wrapped and (d) compensated unwrapped phase image of the squares with phase shifts of 4, 6, and 8 rad. (f) Comparison of the values along the black line in (d) with the reference QPI values obtained without the diffuser.

than 2π, the algorithm was mostly successful in the phase unwrapping (it depended also on the quality of focusing). There was obviously some evidence about the character of the phase changes at the square edge; therefore, the unwrapping was correct. In the case of an abrupt change, there is no certainty about the correct phase. However, it is possible to verify it by another measurement, e.g., with two different central wavelengths and to use the results for the multiwavelength digital holography.[25] CCHM is an achromatic system allowing this kind of measurement.

Imaging of the phase object through a weak diffuser is presented in Fig. 4. Figure 4(a) illustrates the wrapped image phase; Fig. 4(c) depicts the unwrapped and compensated image phase of the object with phase shifts of 0.1, 0.35, and 4 rad. The phase distribution along the black line is compared with that obtained by CCHM without the diffuser [Fig. 4(e)]. Similarly, Fig. 4(b) illustrates the wrapped image phase, while Fig. 4(d) shows the unwrapped and compensated image phase of squares with phase shifts of 4, 6, and 8 rad through the weak diffuser. Fig. 4(f) compares the measured phase along the black line in Fig. 4(d) with and without a diffuser. The third and fourth columns of Table 1 sum up the mean phases φ_m and the standard deviations σ of the phases measured in the interior of the biggest squares in Figs. 4(c) and 4(d). It is clear from Fig. 4 and Table 1 that

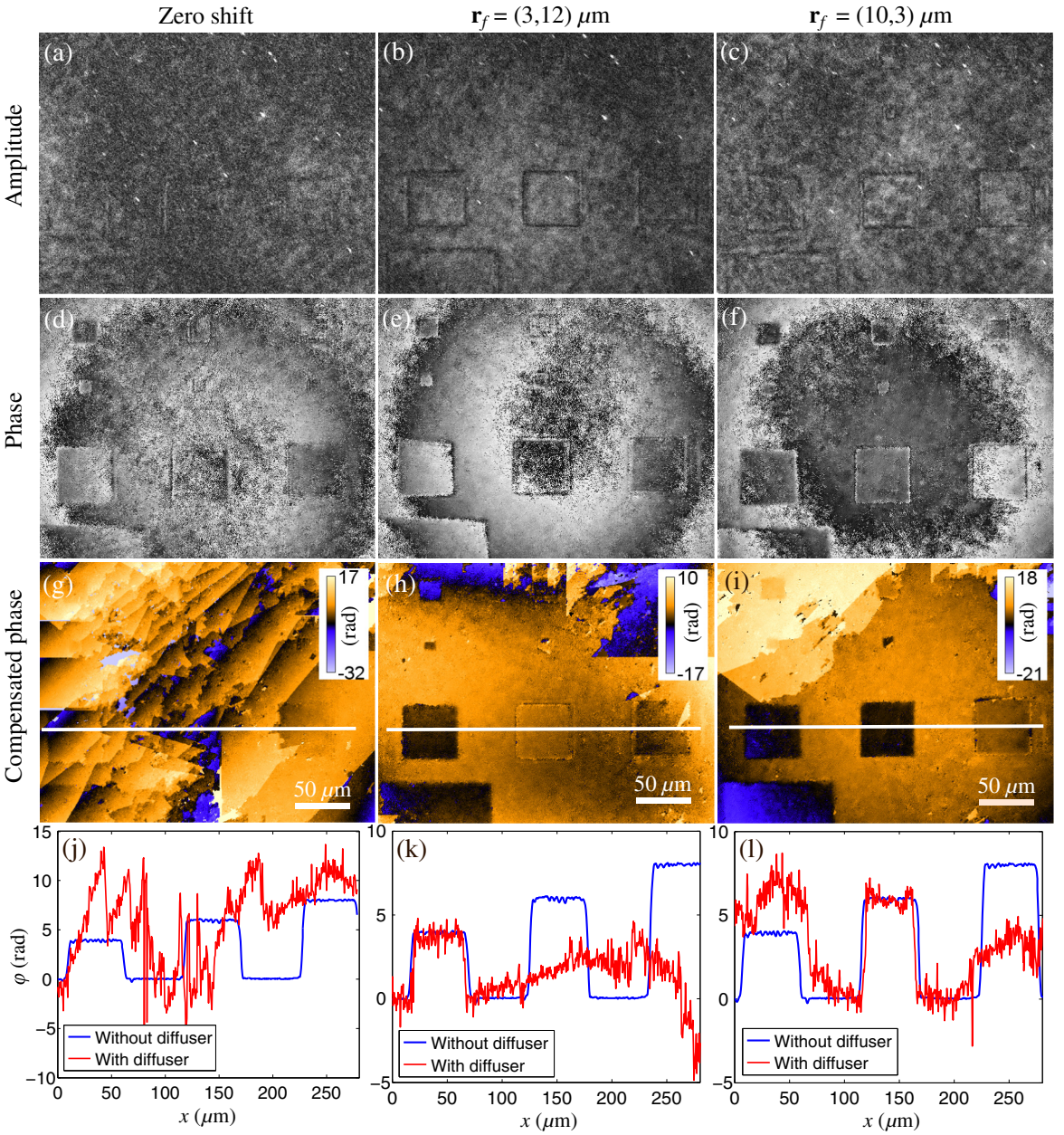

Fig. 5 Experimental verification of QPI of square objects introducing phase shifts 4, 6, and 8 rad through a strong diffuser. The reconstructed amplitude image $|u|$ for (a) $\mathbf{r}_f = (0,0)\ \mu$m, (b) $\mathbf{r}_f = (3,12)\ \mu$m, and (c) $\mathbf{r}_f = (10,3)\ \mu$m. The wrapped phase image for (d) $\mathbf{r}_f = (0,0)\ \mu$m, (e) $\mathbf{r}_f = (3,12)\ \mu$m, and (f) $\mathbf{r}_f = (10,3)\ \mu$m. The compensated unwrapped phase image for (g) $\mathbf{r}_f = (0,0)\ \mu$m, (h) $\mathbf{r}_f = (3,12)\ \mu$m, and (i) $\mathbf{r}_f = (10,3)\ \mu$m. (j) to (l) Comparison of the phase values obtained without the diffuser with the values along the white line in (g) to (i).

the phase shifts of 0.35 rad and greater are imaged well, however, with a higher standard deviation of the phase. Finer details are lost, as obvious for the phase of 0.098 rad. The QPI is possible in the whole field of view without difficulties and the best image is always formed by ballistic light.

Imaging through a strong diffuser is presented in Fig. 5. Figures 5(a)–5(c) are the reconstructed amplitudes, Figs. 5(d)–5(f) are the wrapped phases, Figs. 5(g)–5(i) are compensated unwrapped phases, and Figs. 5(j)–5(l) are phase distributions along the white line in Figs. 5(g)–5(i) compared with the values obtained by CCHM without the diffuser. The first column corresponds to the zero mutual shift $\mathbf{r}_f$ (imaging by means of the ballistic light); the second and third columns show imaging by means of diffuse light with a shift of $r_f = (3,12)\ \mu$m and $r_f = (10,3)\ \mu$m, respectively. In the experiments, $\mathbf{r}_f$ was realized by the shift of the reference objective lens.

In the case of imaging through strongly scattering media, the reconstructed amplitude is weak and more noisy. The areas with a weak reconstructed amplitude correspond to the areas with high phase noise.[26] If the phase differences in the adjacent points due to noise are greater than π, the 2π shifts of the wrapped phase corresponding to the image are badly localizable. The unwrapping then fails, the compensated phase is destroyed, and information about the image phase is lost [see Figs. 5(a), 5(d), and 5(g)]. This is equivalent to the situation when the function w_D does not exhibit a significant principal maximum.

However, as discussed in Sec. 3, CCHM makes it possible to change the quality of the function w_D (and therefore also of the image) by the mutual shift $\mathbf{r}_f$ of the reference and object beam at the output plane. Then, in the region with the good-quality function w_D, the local improvements of the modulus of amplitude, Figs. 5(b)–5(c), and decrease of the amount of the noise in the wrapped phase, Figs. 5(e)–5(f), appear. Then, the phase can be unwrapped and compensated more successfully [see Figs. 5(e), 5(f), 5(h), and 5(i)]. The measurement is influenced by a greater error than in the case of weak diffuser; however, the mean values are relevant [see the regions $x = (0:100)\,\mu$m in Fig. 5(k) and $x = (100:200)\,\mu$m in Fig. 5(l)]. This region of the QPI quality is surrounded by a part of field in which the phase is unwrapped and visualized, however is not relevant [see the regions $x = (125:260)\,\mu$m in Fig. 5(k) and $x = (0:100)\,\mu$m and $x = (200:280)\,\mu$m um in Fig. 5(l)]. Some parts of Figs. 5(h) and 5(i) cannot be unwrapped because the quality of the function w_D is not sufficient here.

Figure 6 illustrates the amplitude and phase imaging through a weak diffuser placed 0.8 mm behind the sample for the case of spatially incoherent light, and almost fully coherent light. Figures 6(a)–6(c) present reconstructed amplitude, wrapped phase, and compensated unwrapped phase, respectively, observed by means of CCHM without a diffuser and with spatially incoherent light. In the other cases, a weak diffuser was used. Figures 6(d)–6(f) show the reconstructed amplitude [Fig. 6(d)], wrapped phase [Fig. 6(e)], and compensated wrapped phase [Fig. 6(f)] with spatially incoherent light. In both cases, the changeable aperture was fully open and the illuminating beam filled the condenser pupil, i.e., $NA = NA_S = 0.3$; the exposure time was 100 ms. The measured phase [Fig. 6(f)] was comparable to the results [Fig. 6(c)] for all three square objects [see Table 1]. Figures 6(g)–6(i) illustrate the amplitude, wrapped, and compensated unwrapped image phase with increased spatial coherence of light. The area of the aperture was reduced to 0.1%, which corresponds to $NA_S = 0.02$; the exposure time was 8 s. The speckles visible in Fig. 6(g) made unwrapping of the image phase [Fig. 6(h)] impossible. Obviously, the spatially incoherent light can significantly improve the quality of the obtained CCHM image due to the coherence gating effect (in contrast to the spatially coherent illumination) and thus make QPI possible also through scattering media.

5 Experiment with Living Cells

CCHM is primarily used for experiments with biological objects. The coherence gating effect makes possible observation of these objects when they are treated in turbid or stationary scattering media. The time-lapse QPI of colorectal carcinoma cells by CCHM and corresponding unwrapped phase images are shown in Fig. 7. Living cells under the 4-mm-thick layer of 0.15% bioactive phospholipid emulsion (BAP) in the cultivation medium are barely visible in the Zernike phase contrast, while in CCHM QPI, one can recognize intracellular

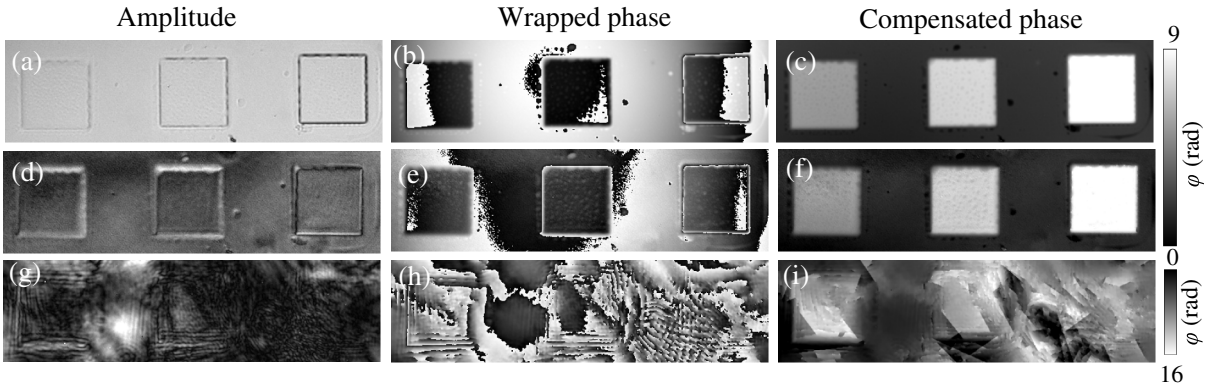

Fig. 6 Experimental verification of amplitude imaging and quantitative phase imaging through a weak diffuser in dependence on the spatial coherence of light. Observation of a square object defined by phase shifts of 4, 6, and 8 rad and the square side length of 50 μm is presented. (a) to (c) Amplitude, wrapped phase, and compensated unwrapped phase observed without the diffuser. (d) to (f) Amplitude, wrapped phase, and compensated unwrapped phase observed with the diffuser in spatially incoherent light, $NA = NA_S = 0.3$. (g) to (i) Amplitude, wrapped phase, and compensated unwrapped phase observed with a diffuser and spatially coherent light, $NA_S = 0.02$.

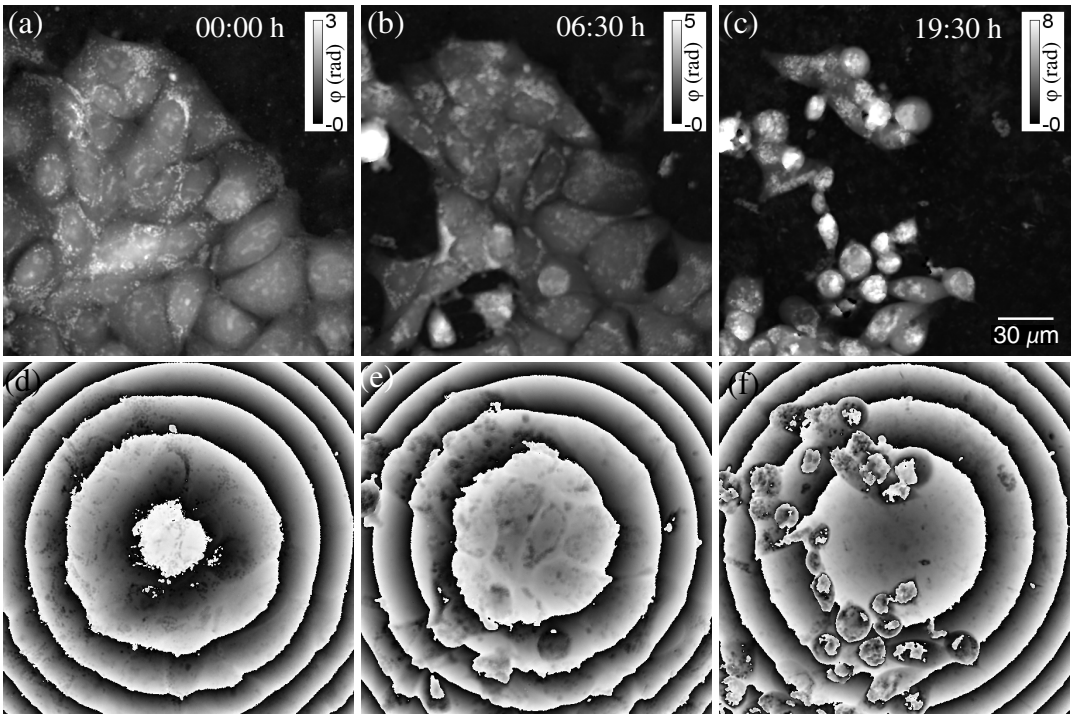

Fig. 7 Colorectal carcinoma cells DLD1 treated with bioactive phospholipids (0.15% bioactive phospholipid emulsion) with anticancer properties emulsified in growth medium. The cells were observed under a 4-mm-thick layer of turbid medium: (a) just after the application and (b) after 6.5 h of exposure. (c) Final situation showing dying cells after 19.5 h. In the calibration scale, 1 rad is equivalent to 0.57 pg/μm^2. (d), (e), and (f) demonstrate corresponding wrapped phase reconstructed from the holograms for the cases (a), (b), and (c).

components. In the series, it is clearly seen that BAP affects not only the cells at the colony edge, but also the cells inside the colony are hit almost at the same time. This indicates that BAP strikes cancer cells indiscriminately of the protection provided by full contact with neighbor cells. A halogen lamp with interference filter 650 nm with FWHM 10 nm, objective lenses $20\times/0.5$, and spatially incoherent light characterized by $\mathrm{NA}_S = 0.29$ were used in the experiment.

6 Conclusion

This study presents a mathematical description of 2-D object imaging through a thin phase scattering layer by means of CCHM. The results of quantitative phase imaging were numerically simulated and experimentally verified for a weak and strong diffuser characterized by a different ratio of amounts of ballistic and diffuse light. The paper has shown that the phase image can be formed both by ballistic and diffuse light, depending on the diffuser properties. In the case of a weak diffuser, the best signal is always determined by the ballistic light, with resolution comparable or slightly worse than without the diffuser. The quality of the image behind a strong diffuser depends on the mutual shift $\mathbf{r}_f$ of the reference and object beam images at the output plane. In some cases, the object can be imaged by both ballistic ($\mathbf{r}_f = 0$) and diffuse ($\mathbf{r}_f \neq 0$) light, and in other cases by the diffuse light only with surprisingly good image quality. The signal is, however, more noisy, the resolution worse, and in some cases, the imaging can be rather a phase visualization technique. Even the best choice of $\mathbf{r}_f$ can usually lead to a good-quality QPI in a limited area of the image field. However, this area can be extended recombining images for several $\mathbf{r}_f$.

The authors have also demonstrated the influence of the degree of spatial coherence on the quality of the image created through a thin scattering layer, for weak and strong diffusers. The numerical simulations and experimental results confirm the benefits of the spatially incoherent light for imaging through scattering media by means of CCHM. The results can be useful in biomedical applications and research, for example, for assessment of reactions of carcinoma cells to various drugs, which exhibit scattering properties.

Acknowledgments

This work was supported by the project EXCELLENT TEAMS (CZ.1.07/2.3.00/30.0005) from European Social Fund, "CEITEC—Central European Institute of Technology" (CZ.1.05/1.1.00/02.0068) from European Regional Development Fund, and by the project 15-14612S from the Czech Science Foundation.

References

1. I. Freund, "Looking through walls and around corners," *Phys. A* **168**(1), 49–65 (1990).
2. O. Katz et al., "Focusing and compression of ultrashort pulses through scattering media," *Nat. Photon.* **5**, 372–377 (2011).
3. J. Bertolotti et al., "Non-invasive imaging through opaque scattering layers," *Nature* **491**(7423), 232–234 (2012).
4. M. Vellekoop and C. M. Aegerter, "Scattered light fluorescence microscopy: imaging through turbid layers," *Opt. Lett.* **35**(8), 1245–1247 (2010).

5. H. P. Baltes, *Inverse Scattering Problems in Optics*, Springer-Verlag, Berlin (1980).
6. C. Dunsby and P. M. W. French, "Techniques for depth-resolved imaging through turbid media including coherence-gated imaging," *J. Phys. D: Appl. Phys.* **36**, 207–227 (2003).
7. V. T. Willwacher et al., "Recovering three-dimensional shape around a corner using ultrafast time-of-flight imaging," *Nat. Commun.* **3**, 745 (2012).
8. M. Sticker et al., "Quantitative differential phase measurement and imaging in transparent and turbid media by optical coherence tomography," *Opt. Lett.* **26**(8), 518–520 (2001).
9. P. Marquet et al., "Digital holographic microscopy: a noninvasive contrast imaging technique allowing quantitative visualization of living cells with subwavelength axial accuracy," *Opt. Lett.* **30**(5), 468–470 (2005).
10. G. Popescu et al., "Erythrocyte structure and dynamics quantified by Hilbert phase microscopy," *J. Biomed. Opt.* **10**(6), 060503 (2005).
11. W. C. Warger, II et al., "Phase-subtraction cell-counting method for live mouse embryos for live mouse embryos beyond the eight-cell stage," *J. Biomed. Opt.* **13**(3), 034005 (2008).
12. H. Janeckova, P. Vesely, and R. Chmelik, "Proving tumour cells by acute nutritional/energy deprivation as a survival threat: a task for microscopy," *Anticancer Res.* **29**(6), 2339–2345 (2009).
13. J. Balvan et al., "Multimodal holographic microscopy: distinction between apoptosis and oncosis," *PLoS One* **10**(3), e0121674 (2015).
14. E. Leith et al., "Imaging through scattering media with holography," *J. Opt. Soc. Am. A* **9**(7), 1148–1153 (1992).
15. S. Li and J. Zhong, "Dynamic imaging through turbid media based on digital holography," *J. Opt. Soc. Am. A* **31**(3), 480–486 (2014).
16. M. Paturzo et al., "Microscopy imaging and quantitative phase contrast mapping in turbid microfluidic channels by digital holography," *Lab Chip* **12**(17), 3073–3076 (2012).
17. V. Bianco et al., "Clear coherent imaging in turbid microfluidics by multiple holographic acquisitions," *Opt. Lett.* **37**(20), 4212–4214 (2012).
18. R. K. Singh, A. M. Sharma, and B. Das, "Quantitative phase-contrast imaging through a scattering media," *Opt. Lett.* **39**(17), 5054–5057 (2014).
19. S. Tamano, Y. Hayasaki, and N. Nishida, "Phase-shifting digital holography with a low-coherence light source for reconstruction of a digital relief object hidden behind a light-scattering medium," *Appl. Opt.* **45**(5), 953–959 (2006).
20. T. Slabý et al., "Off-axis setup taking full advantage of incoherent illumination in coherence-controlled holographic microscope," *Opt. Express* **21**(12), 14747–14762 (2013).
21. M. Lošt'ák et al., "Coherence-controlled holographic microscopy in diffuse media," *Opt. Express* **22**(4), 4180–4195 (2014).
22. R. Chmelik et al., "The role of coherence in image formation in holographic microscopy," *Prog. Opt.* **59**, 267–335 (2014).
23. R. M. Goldstein, H. A. Zebken, and C. L. Werner, "Satellite radar interferometry: two-dimensional phase unwrapping," *Radio Sci.* **23**(4), 713–720 (1988).
24. .T. Zikmund et al., "Sequential processing of quantitative phase images for the study of cell behavior in real-time digital holographic microscopy," *J. Microsc.* **256**(2), 117–125 (2014).
25. J. Gass, A. Dakoff, and M. K. Kim, "Phase imaging without 2π ambiguity by multiwavelength digital holography," *Opt. Lett.* **28**(13), 1141–1143 (2003).
26. J. W. Goodman, *Statistical Optics*, Wiley-Interscience, New York, pp. 498–500 (2000).

Vera Kollarova is a postdoctoral fellow at Brno University of Technology in the Czech Republic. She received her BS and MS degrees in optics from Palacký University in Olomouc in 2001 and 2003, respectively, and a PhD in optics from the same university in 2011. Her current research interests include holographic microscopy and imaging through scattering media.

Jana Collakova is a PhD student at the Brno University of Technology. She received her BS degree in optics from the Palacky University in Olomouc in 2009 and her MS degree in optics and precise mechanics from the Brno University of Technology in 2011. Her current research interests include digital holographic microscopy in turbid media and living cells imaging.

Zbynek Dostal is a PhD student at the Brno University of Technology. He received his BS degree in mechanical engineering in 2007 and his MS degree in optics and precise mechanics in 2009 from the Brno University of Technology. He is a co-author of the CCHM patent for which he received the Werner von Siemens Excellence Award 2013. His current research interests include holographic microscopy, automation in microscopy, optical and mechanical design.

Pavel Vesely is a senior research scientist at the CEITEC, Brno University of Technology. He received his MD degree from the Charles University in Prague in 1961 and his PhD in experimental biology from the Czechoslovak Academy of Sciences in 1965. He is the author of more than 100 journal papers. His life long research interests in cancer cell biology currently include domestication of coherence controlled holographic microscopy in cell biology research.

Radim Chmelik is a professor of applied physics at the Brno University of Technology. He received his MS degree in solid state physics from the Masaryk University in Brno, in 1989 and his PhD in physical and materials engineering from the Brno University of Technology in 1997. He is the author of more than 40 journal papers. His current research interests include wave optics, imaging theory, advanced and 3D light microscopy, and holographic microscopy.